Lattice-parameter changes and triclinic distortions in $Li_xMo_6Se_8$ for $0<x<4$

J. R. Dahn, W. R. McKinnon, and S. T. Coleman*
Solid State Chemistry, Division of Chemistry, National Research Council of Canada, Ottawa, Ontario, Canada K1A 0R9
(Received 14 June 1984)

Using *in situ* x-ray diffraction we have measured the room-temperature structure of $Li_xMo_6Se_8$ for $0<x<4$. We find four single-phase regions: two rhombohedral phases and two triclinic phases. All of the structural changes are reversible with x. Features in the voltage of $Li/Li_xMo_6Se_8$ electrochemical cells are associated with each of the structural changes.

INTRODUCTION

The Chevrel phases are ternary molybdenum chalcogenides ($A_xMo_6X_8$; A=metal, X=chalcogen) with structures and properties that depend on A and x.[1,2] Most have rhombohedral structures at room temperature and many distort to triclinic structures at low temperature. These distortions influence other properties, notably superconductivity, and have therefore received much study.[3,4]

Early work on $Li_xMo_6Se_8$ (Ref. 5), showed that x can vary between 0 and 4. Later studies[6] showed that $Li_xMo_6Se_8$ has a rhombohedral structure for $x=0$, 1, 3, and 3.2 at room temperature, with an unidentified structural distortion for $x>3.6$. Recently,[7] we showed that $Li_xMo_6Se_8$ is single phase at room temperature for $0<x<1$ and reported the variation with x ($0<x<1$) of the rhombohedral lattice parameters.

Here we report the room-temperature structure of $Li_xMo_6Se_8$ for $0<x<4$. We give details of our earlier experiments for $0<x<1$ (Ref. 7) and present new results for $1<x<4$. $Li_xMo_6Se_8$ was prepared by intercalating Li into Mo_6Se_8 in electrochemical cells with beryllium x-ray windows.[8] Thus, x could be changed *in situ* by charging or discharging the cell in an x-ray diffractometer. There are four distinct single-phase regions for $0<x<4$: two rhombohedral and two triclinic phases. We have measured the variation of the lattice parameters in each of these phases. Our technique allows us to study the reversibility of the structure to changes in x, and we find that each of the rhombohedral-triclinic distortions is reversible. We also show the correlation between the structural phase transitions and features in the voltage, $V(x)$, and $-dx/dV$ of $Li/Li_xMo_6Se_8$ electrochemical cells.

EXPERIMENTAL

Mo_6Se_8 was prepared from Mo foil (99.999% purity) and Se pellets (99.99% purity). Quartz ampoules containing the elements and 250 Torr of argon were sealed, then held at 1250°C for 60 h. The rhombohedral lattice parameters of our Mo_6Se_8, $a=6.658$ Å and $\alpha=91.76°$, are in good agreement with other results.[9]

We measured $V(x)$ in $Li/Li_xMo_6Se_8$ cells as described earlier.[10,11] The cells were charged or discharged with a constant current while V was monitored as a function of time.[10] In this method, changes in x are proportional to changes in time and $-dx/dV$ is calculated by numerically differentiating $V(x)$.

In situ x-ray diffraction experiments were made as in (Ref. 8) except that a Stoe Bragg-Brentano diffractometer controlled by a computer was used instead of a Philips instrument. The homogeneously intercalated samples are prepared by fixing V and waiting for equilibrium. Then x-ray diffraction data are collected before the voltage is stepped to a new value. x is determined either by monitoring the charge transferred to the intercalation electrode during the equilibration or from $V(x)$.

It is difficult to align the cathodes of *in situ* x-ray cells exactly on the axis of the goniometer.[8] This off-axis displacement shifts Bragg peaks from their ideal angles. The data shown in Figs. 6, 7, and 9 are not corrected for this displacement (the correction is about 0.05° at $2\theta=60°$) but the Bragg angles used in least-squares refinements for the lattice parameters are corrected, as are the angles in Table I.

RESULTS

Structure of $Li_xMo_6Se_8$ for $0<x<1$

Figure 1 shows $V(x)$ measured for the first discharge and charge of a $Li/Li_xMo_6Se_8$ cell at 28°C. x was determined directly from the mass of the intercalation cathode and the charge transfer. The behavior in Fig. 1 is typical of $Li/Li_xMo_6Se_8$ cells and agrees well with data measured by Tarascon *et al.*[6] The currents used correspond to a change $\Delta x=1$ in 25 h. The results for the charge do not return $x=0$ in Fig. 1 probably because some $Li_xMo_6Se_8$ has become electrically disconnected from the cathode and because of a small side reaction for voltages near 1.7 V (see below).

A prominent feature in Fig. 1 is the abrupt drop in voltage near $x=1$. Such a drop is expected when Li completely fills one type of site and begins to occupy another. For $x<1$, α is less than 92°. Yvon[1] has found that in this range of α, A atoms in $A_xMo_6X_8$ generally occupy sites on the $\bar{3}$ axis. There is one such site per Mo_6X_8 unit so at $x=1$ all such sites are full and the voltage drops.

For $0<x<1$, $V(x)$ for $Li/Li_xMo_6Se_8$ cells is well described by a mean-field theory[7] which assumes that Li

TABLE I. Results of a lattice-parameter refinement for $Li_4Mo_6Se_8$.

$a=6.908(1)$ Å, $\alpha=95.828°$
$b=6.938(1)$ Å, $\beta=91.645°$
$c=6.980(1)$ Å, $\gamma=96.794°$

h	k	l	Observed 2θ (deg)	Calculated 2θ (deg)	Calculated plane spacing (Å)
1	1	1	24.334	24.33	3.658
0	0	2	25.698	25.68	3.469
2	0	0	26.003	26.00	3.427
0	2	0	26.003	26.01	3.425
2	$\bar{1}$	0	27.642	27.65	3.226
2	0	$\bar{1}$	28.566	28.57	3.124
2	0	1	29.576	29.54	3.023
$\bar{1}$	1	2	31.789	31.75	2.818
2	1	1	34.209	34.21	2.621
$\bar{2}$	0	2	36.065	36.07	2.490
2	$\bar{2}$	1	36.503	36.49	2.462
1	2	$\bar{2}$	38.051	38.04	2.365
$\bar{2}$	1	2	38.312	38.31	2.350
3	0	0	39.450	39.44	2.285
1	$\bar{3}$	0	40.072	40.07	2.250
1	0	$\bar{3}$	40.647	40.66	2.219
2	1	2	41.982	41.97	2.153
1	2	2	42.516	42.52	2.126
$\bar{1}$	3	1	43.383	43.38	2.086
3	1	$\bar{1}$	44.345	44.34	2.043
3	$\bar{2}$	1	46.539	46.55	1.951
1	3	$\bar{2}$	48.297	48.29	1.884
$\bar{2}$	1	3	48.695	48.69	1.870
2	2	2	49.853	49.86	1.829
1	$\bar{4}$	0	53.551	53.55	1.711
1	$\bar{1}$	4	55.008	55.01	1.669
$\bar{1}$	4	1	56.602	56.61	1.626
4	1	$\bar{1}$	57.714	57.72	1.597

occupies only one type of site in Mo_6Se_8. Figure 2 shows an example of $V(x)$ and $-dx/dV$ at 38 °C. The charge and discharge have over 200 data points, which we have joined by straight lines. The measured change in x from 2.30 to 2.00 V was $\Delta x=0.90$ for this cell. To correct for $Li_xMo_6Se_8$ which is electrically disconnected from the cathode, we normalize the values of x to $x=0$ and 1 at 2.3 and 2.0 V, respectively. The currents correspond to a change $\Delta x=1$ in 50 h. The good agreement between charge and discharge shows the cell is near equilibrium and demonstrates the reversibility of intercalation for $0<x<1$. The solid curve in Fig. 2(b) is the mean-field prediction.[7]

The mean-field theory in (Ref. 7) predicts that $Li_xMo_6Se_8$ is a single phase at room temperature. We have confirmed this as follows. Figure 3 shows portions of x-ray diffraction profiles taken at 22 °C on the same cell at several values at x. The Bragg peaks shift in angle as x changes but do not change in width. At each x the diffraction profiles show a single phase. Figure 4 shows the variation of the rhombohedral lattice parameters for $0<x<1$ determined from least-squares refinements to the positions of at least 20 Bragg peaks. The changes in structure were found to be fully reversible. The linear lattice expansion in this compound leads to the long-ranged attractive interaction between lithium atoms discussed previously.[7]

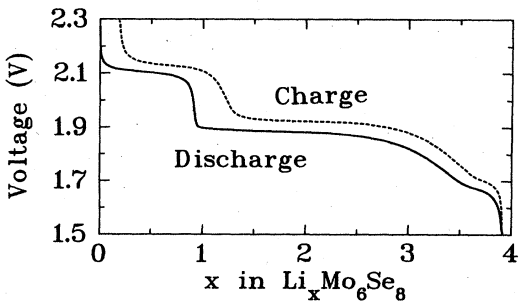

FIG. 1. $V(x)$ for a Li/$Li_xMo_6Se_8$ cell at 28 °C.

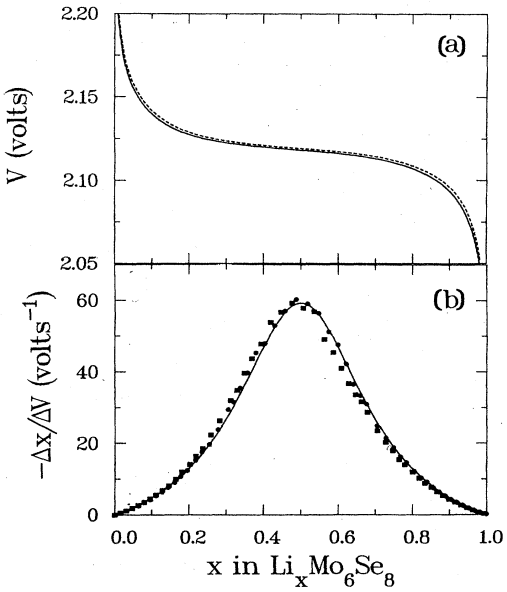

FIG. 2. (a) $V(x)$ for a $Li/Li_xMo_6Se_8$ cell at 38 °C; the solid line denotes discharge, and the dashed line denotes charge. (b) $-dx/dV$ versus x from (a). The filled square denotes discharge, and the filled circle denotes charge. The solid curve is the theoretical prediction of Ref. 7.

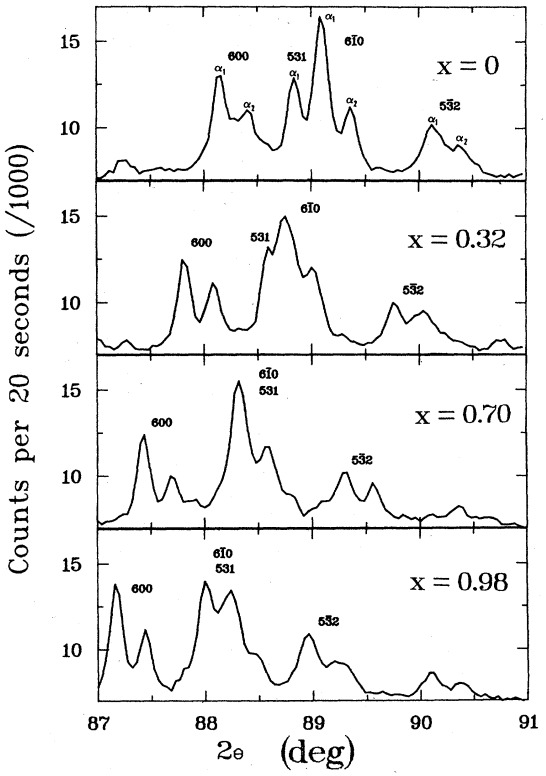

FIG. 3. X-ray diffraction profiles of $Li_xMo_6Se_8$ taken at $x=0$, 0.32, 0.70, and 0.98. The peaks are labeled by their rhombohedral Miller indices.

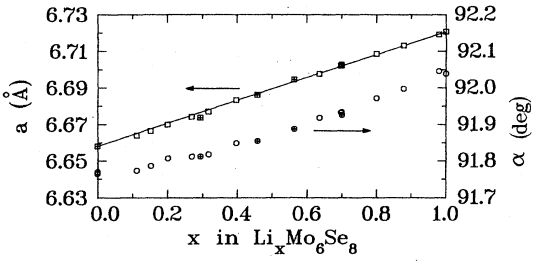

FIG. 4. Variation of the lattice parameters a (squares) and α (circles) of $Li_xMo_6Se_8$ as determined by *in situ* x-ray diffraction. Open symbols were measured on discharge; symbols with crosses on charge.

Structure of $Li_xMo_6Se_8$ for $1<x<4$

For $0<x<1$, $Li_xMo_6Se_8$ is a single phase, which we call R_1, with a rhombohedral structure. In contrast, there are three different phases for $x>1$, one rhombohedral structure (R_2) and two triclinic structures (T_1 and T_2).

Transitions between these phases appear as peaks in $-dx/dV$. Figure 5 shows $-dx/dV$ for a $Li/Li_xMo_6Se_8$ cell at 28 °C. The peaks near 1.90, 1.88, and 1.69 V correspond, respectively, to the transitions $R_1 \leftrightarrow T_1$, $T_1 \leftrightarrow R_2$, and $R_2 \leftrightarrow T_2$. In contrast, the peak at 2.1 V is not a phase transition; it is the behavior of the single phase R_1.

The large peak in Fig. 5 near 1.90 V corresponds to a first-order phase transition between the rhombohedral phase R_1 with $x=1$ and the triclinic phase T_1 with $x \simeq 2.5$. The smaller peak at 1.88 V corresponds to a first-order transition between the T_1 phase and the rhombohedral phase R_2. During such first-order transitions an x-ray diffraction profile shows two sets of Bragg peaks, one for each of the two coexisting phases. As an example, Fig. 6 shows portions of x-ray diffraction profiles taken

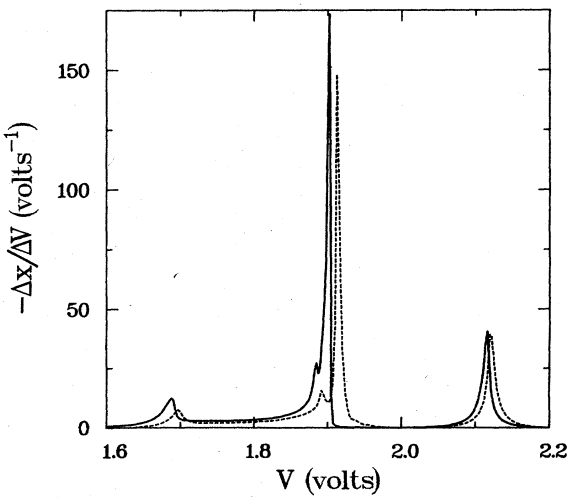

FIG. 5. $-dx/dV$ versus V for a $Li/Li_xMo_6Se_8$ cell at 28 °C. The currents used corresponded to a change of $\Delta x=1$ in 25 h. The $-dx/dV$ scale was determined from the currents used and the cathode mass and has not been adjusted in any way.

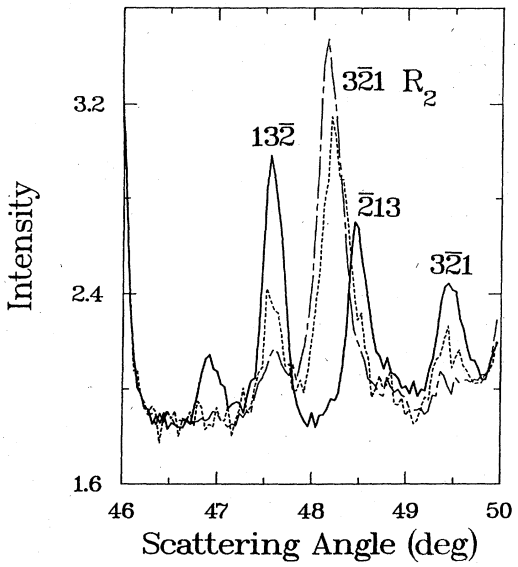

FIG. 6. Portions of x-ray diffraction profiles near the $T_1 \leftrightarrow R_2$ transition. Solid line: T_1 phase at 1.890 V; long-dashed–short-dashed line: R_2 phase at 1.870 V; dashed lined: coexistence of T_1 and R_2 phases near 1.880 V. The Miller indices of the T_1 and R_2 peaks are indicated.

near the $T_1 \leftrightarrow R_2$ transition. The 3$\bar{2}$1 peak, like each of the strong Bragg peaks in the R_2 phase (except 111, 222, etc.), splits into three peaks of about $\frac{1}{3}$ the intensity in the T_1 phase. This splitting arises because the triclinic distortion destroys the threefold symmetry axis of the rhombohedral phase. Thus peaks like 3$\bar{2}$1, $\bar{2}$13, and 13$\bar{2}$ (cyclic permutations), which have the same Bragg angle and intensity in the R_2 phase, have different angles in the T_1 phase. Because the intensities of the triplet peaks are each about $\frac{1}{3}$ the intensity of the R_2 parent peaks, the atom positions within the unit cell must not change radically.

The peak near 1.7 V in Fig. 5 corresponds to a transition from the R_2 phase to a second triclinic phase T_2. Again each R_2 Bragg peak splits into three peaks, signifying a triclinic distortion (Fig. 7). The transition does not appear to be first order because coexisting R_2 and T_2 phases are not observed. Instead, the x-ray intensity shifts smoothly from the R_2 peaks to the T_2 peaks as the transition proceeds. However, near the transition we were unable to index the pattern because of poorly revolved peaks, so we have no proof that the transition is continuous. The *in situ* technique makes indexing the distorted structure much easier when peaks split smoothly like this, because each peak can be traced back to its parent peak in the undistorted structure.

Figure 8 shows the lattice parameters and unit cell

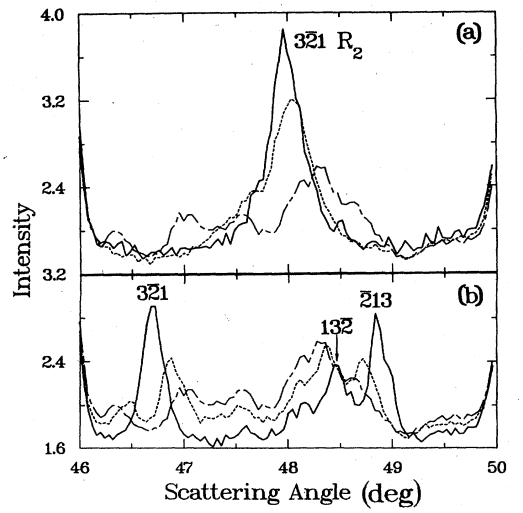

FIG. 7. Portions of x-ray diffraction profiles near the $R_2 \leftrightarrow T_2$ transition. (a) Solid line: 1.710 V; dashed line: 1.697 V; long-dashed–short-dashed line: 1.690 V. (b) Long-dashed–short-dashed line: 1.690 V; dashed line: 1.685 V; solid line: 1.600 V. The Miller indices of the R_2 and T_2 peaks are indicated.

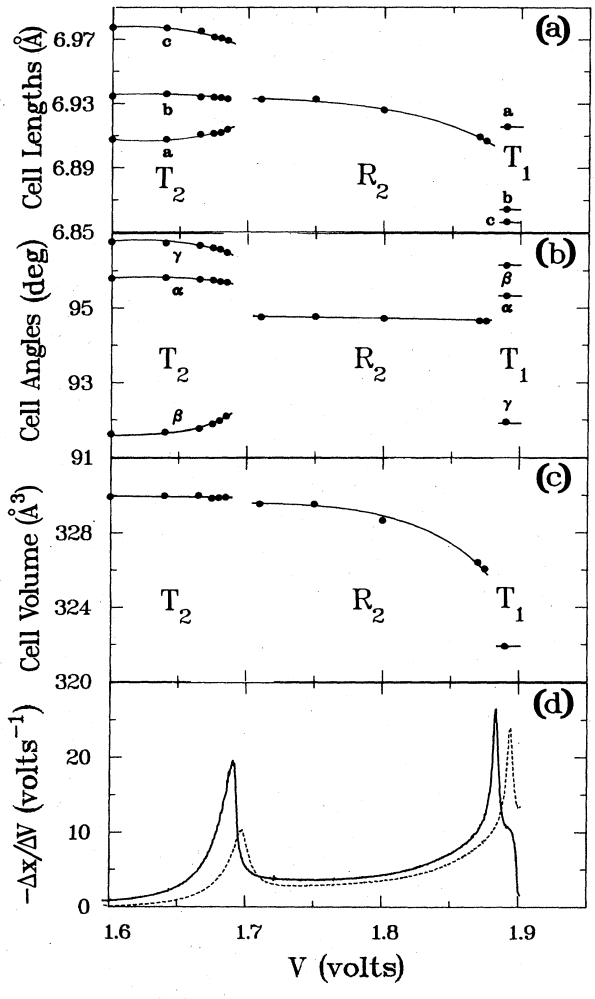

FIG. 8. (a) Unit cell lengths, (b) unit cell angles, (c) unit cell volume of $Li_xMo_6Se_8$, and (d) $-dx/dV$ of $Li/Li_xMo_6Se_8$ cells plotted versus V. The solid lines in (a), (b), and (c) are guides to the eye. The T_1, R_2, and T_2 phases are indicated. In (d), the solid curve is for the discharge and the dashed curve is for the charge.

volume of $Li_xMo_6Se_8$ and $-dx/dV$ of $Li/Li_xMo_6Se_8$ cells plotted versus V. The structural data in Fig. 8 were obtained by fixing the cell at successively lower voltages, so the structural data should be compared to $-dx/dV$ for the discharge. This figure shows that the distortions occur at the peaks in $-dx/dV$. The data in Fig. 8(d) is from a charge and discharge of a $Li/Li_xMo_6Se_8$ cell between 1.6 and 1.9 V, using currents which took 50 h to change x by $\Delta x=1$. The $T_1 \leftrightarrow R_1$ transition starts at 1.908 V; cells charged to 1.900 V are in the T_1 phase.

Table I shows the results of a typical refinement to obtain the lattice parameters of the T_2 phase. Figure 9(a) shows a calculated powder pattern for $Li_4Mo_6Se_8$, which can be compared to the data in Fig. 9(b). The calculation assumes that the Mo and Se atoms have the same fractional atomic coordinates as in Mo_6Se_8 (Ref. 1) and analytic approximations for their atomic scattering factors were taken from the *International Tables for X-ray Crystallography*.[13] Gaussian peaks of halfwidth $\Delta 2\theta=0.20°$ were used in the calculation. The shaded peaks in Fig. 9(b) are peaks from the cell components, not $Li_xMo_6Se_8$. We have not attempted to obtain the atom positions from Rietveld[14] profile refinements. Even so, the good agreement shown in Fig. 9 indicates that the fractional atomic coordinates in the T_2 phase are close to those of Mo_6Se_8. Similar agreement was obtained in calculations for the R_1, T_1, and R_2 phases.

Room-temperature lattice parameters of $Li_xMo_6Se_8$ versus x (Fig. 10) were obtained from Fig. 8 and $V(x)$ for discharging cells. Here, the errors in our determination of x are much greater than those in Fig. 4, which were about 2%. This is because our $Li/Li_xMo_6Se_8$ cells always took longer to discharge than to charge (using the same currents) when cycled between 1.6 and 1.9 V. In Fig. 8(d), for example, the integral under the discharge (which gives Δx) is larger than the integral under the charge; most of this difference is in the peak near 1.7 V. (The same cell design and electrolyte gave 100% Coulombic efficiency in similar experiments on other Li intercalation systems.[10,15]) This difference between charge and discharge implies that there are side reactions in the cell, principally at low voltages, which consume Li. Since we do not know how the side-reaction current depends on V, we cannot calculate x exactly.

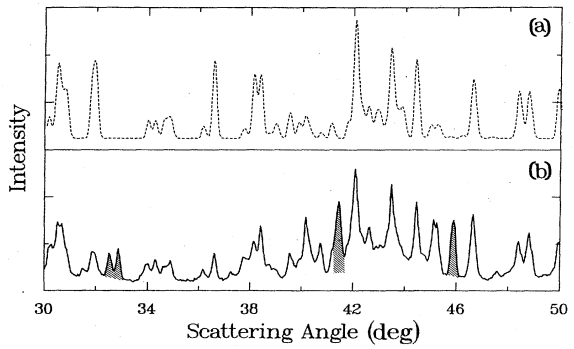

FIG. 9. (a) Calculated and (b) measured powder x-ray diffraction profiles for $Li_4Mo_6Se_8$. See text.

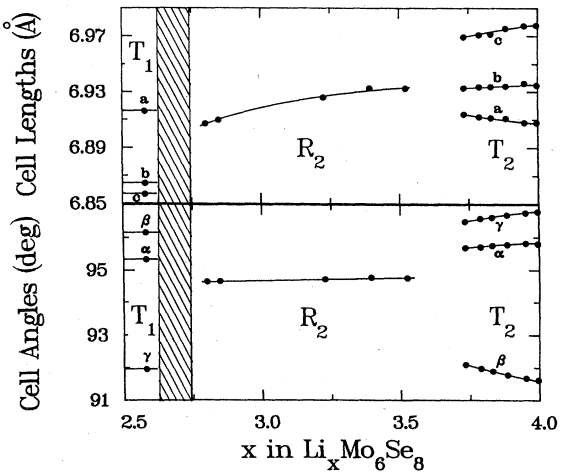

FIG. 10. Lattice parameters of $Li_xMo_6Se_8$ versus x for the T_1, R_2, and T_2 phases. The solid lines through the data points are guides to the eye and the shaded region indicates the coexistence of R_2 and T_1 phases. The boundaries of the shaded region are approximate.

We calculate x in Fig. 10 in two steps. First we fixed $x=0$ at 2.3 V and $x=1$ at 2.0 V, and calculated the value at x for the beginning of the T_1 phase from the average of charges and discharges for several cells. This gives $x=2.5\pm0.2$. We then fixed $x=2.5$ at 1.908 V for the discharge of Fig. 8(d) and $x=4$ at 1.5 V and calculated x. (The value of $x=4$ for the composition of the fully intercalated compound is the maximum value of x seen in other Chevrel compounds[1] and agrees with Fig. 1.) Using the charge from Fig. 8(d) gave slightly different values of x—we estimate the maximum systematic error in x in Fig. 10 to be ±0.3 near $x=3.3$. However, our lattice-parameter data for the R_2 phase is in excellent agreement with the values reported for $x=3$ and $x=3.2$ by Tarascon *et al.*[6] where the Li composition was determined by chemical analysis.

DISCUSSION

The rhombohedral angle α has been shown by Yvon[1] to be sensitive to the amount of delocalization of the A atom in $A_xMo_6X_8$ from the $\bar{3}$ axis. Here, in $Li_xMo_6Se_8$, we find $\alpha<92°$ for $x<1$ and $\bar{\alpha}=(\alpha+\beta+\gamma)/3\simeq95°$ for $x>2.5$. We suggest that the lithium is fairly well localized in the sites at the origin of the Mo_6Se_8 unit cell (on the $\bar{3}$ axis) for $x<1$ and is delocalized into sites similar to those seen for $Cu_xMo_6S_8$ when $x>2.5$. As x in $Li_xMo_6Se_8$ increases past 1, α must increase in order to make more sites available for Li, because there is only 1 site on the $\bar{3}$ axis when x is small, but 12 positions (which cannot all be simultaneously filled) when α is large.[1] Presumably the large region of coexisting R_1 and T_1 phases reflects the fact that Chevrel compounds with intermediate α are rare.

The triclinic distortions to the T_1 and T_2 phases from the R_2 phase both produce peaks in $-dx/dV$ [Figs. 5

and 8(d)]. This indicates that the lithium is involved in the distortion because the voltage of $Li/Li_xMo_6Se_8$ cells is proportional to the chemical potential of Li in $Li_xMo_6Se_8$.[12] The transitions might be order-disorder transitions involving the intercalated Li. Lithium order-disorder transitions in 2H-Li_xTaS_2 have been previously observed by a study of peaks in $-dx/dV$.[10] For example, the T_1 phase might be similar to the low-temperature triclinic phase of $Cu_2Mo_6S_8$ where copper atoms fill two of the six "inner sites" in an ordered way.[1] In $Cu_2Mo_6S_8$, this breaks the threefold symmetry and causes a triclinic distortion. The transitions might be due to an electronically driven lattice instability as in $EuMo_6S_8$.[4] As Li is added to $Li_xMo_6Se_8$, more electrons are added to the conduction band (in a rigid band picture) which may induce a lattice instability at some Li concentration. Again this should be observed as a peak in $-dx/dV$.

SUMMARY

We have measured the room-temperature structure of $Li_xMo_6Se_8$ for $0<x<4$ and have correlated the structural changes with $V(x)$ and $-dx/dV$ of $Li/Li_xMo_6Se_8$ cells. We find four single-phase regions, two rhombohedral phases, and two triclinic phases. For $0<x<1$, $Li_xMo_6Se_8$ is a single phase with a rhombohedral structure. For $1<x<2.5$, coexisting rhombohedral and triclinic phases are observed. A narrow triclinic single-phase region is found for $2.5<x<2.6$ which coexists with a second rhombohedral phase for $2.6<x<2.75$. This rhombohedral phase exists for $2.75<x<3.5$ and distorts to a second triclinic phase for $x>3.6$. All of the structural changes are reversible with x.

*Present address: University of British Columbia, Vancouver, B.C., Canada.

[1] K. Yvon, in *Current Topics in Materials Science,* edited by E. Kaldis (North-Holland, Amsterdam, 1979), Vol. 3, p. 53.
[2] O. Fischer, Appl. Phys. **16**, 1 (1978).
[3] R. Baillif, A. Dunand, J. Muller, and K. Yvon, Phys. Rev. Lett. **47**, 672 (1981).
[4] R. Baillif, A. Junod, B. Lachal, J. Muller, and K. Yvon, Solid State Commun. **40**, 603 (1981).
[5] R. Schollhorn, M. Kumpers, and J. O. Besenhard, Mater. Res. Bull. **12**, 781 (1977).
[6] J. M. Tarascon, F. J. Disalvo, D. W. Murphy, G. W. Hull, and J. V. Waszczak, J. Solid State Chem. (to be published).
[7] S. T. Coleman, W. R. McKinnon, and J. R. Dahn, Phys. Rev. B **29**, 4147 (1984).
[8] J. R. Dahn, M. A. Py, and R. R. Haering, Can. J. Phys. **60**, 307 (1982).
[9] O. Bars, J. Guillevic, and D. Grandjean, J. Solid State Chem. **6**, 48 (1973).
[10] J. R. Dahn and W. R. McKinnon, J. Electrochem. Soc. **131**, 1823 (1984).
[11] D. C. Dahn and R. R. Haering, Solid State Commun. **44**, 29 (1982).
[12] W. R. McKinnon and R. R. Haering, in *Modern Aspects of Electrochemistry,* edited by R. F. White, J. O. 'M. Bockris, and B. E. Conway (Plenum, New York, 1983), Vol. 15.
[13] *International Tables for X-ray Crystallography,* edited by J. A. Ibers and W. C. Hamilton (Kynoch, Birmingham, 1974), Vol. 4.
[14] H. M. Rietveld, J. Appl. Crystallogr. **2**, 65 (1969).
[15] J. R. Dahn and W. R. McKinnon, Solid State Ionics (to be published).